Detecting resonances in conservative maps using evolutionary algorithms

Y.G. Petalas [a,b], C.G. Antonopoulos [c], T.C. Bountis [c], M.N. Vrahatis [a,b,*]

[a] *Computational Intelligence Laboratory (CI Lab), Department of Mathematics, University of Patras, GR-26110 Patras, Greece*
[b] *University of Patras Artificial Intelligence Research Center (UPAIRC), University of Patras, GR-26110 Patras, Greece*
[c] *Center for Research and Applications of Nonlinear Systems (CRANS), Department of Mathematics, University of Patras, GR-26110 Patras, Greece*

ARTICLE INFO

ABSTRACT

A numerical method is proposed for detecting resonances of conservative maps which reduces this task to an optimization problem. We then solve this problem using evolutionary algorithms, which are methods for global optimization inspired by biological evolution. The proposed methodology is simple and can be easily applied to maps of arbitrary dimensions. In this Letter we apply it to several examples of 2- and 4-dimensional conservative maps, with quite promising results concerning integrability, the location of resonances and the presence of chaotic regions surrounding the island chains that correspond to these resonances.

1. Introduction

Conservative maps, especially symplectic ones, are encountered in many examples of physical significance: Hamiltonian systems, in the vicinity of their fixed points and periodic orbits, lead to Poincare maps which are symplectic [1]. Also the motion of charged particles around magnetic field lines can be described by symplectic maps [2], while such maps are commonly used to study the stability of particle beams in high energy accelerators [3,4].

When conservative maps are integrable their phase space is foliated by smooth invariant surfaces (or tori) on which the motion is always regular (i.e. periodic or quasiperiodic). In most applications, however, these maps are non-integrable and possess *resonances* characterized by chains of islands of regular motion, around which there are domains where the motion is irregular, or chaotic (i.e. extremely sensitive to the choice of initial conditions). It is important, therefore, to develop methods to determine the location and width of these resonances, as well as estimate the size and extent of the chaotic regions around them.

The methodology proposed in this Letter reduces the problem of detecting resonances in $2N$-dimensional conservative maps to a global optimization task, which proceeds as follows: It starts from a central elliptic point of the map (which we translate for convenience to the origin) and considers annular regions around that point, lying between thin "spherical" shells at consecutively increasing radial distances, $r_1 < r < r_2$. Within each of these shells the method searches for a point whose iteration will result in an orbit that maximizes a quantity D, representing the difference between the maximum and minimum distance of the produced orbit from the origin. Next, a plot is generated of $D = D(r)$, as a function of the radial distance r, which is well approximated by a continuous curve, for thin enough spherical shells (e.g. $r_2 - r_1 \simeq 0.001$ up to 0.005). This curve typically starts from values close to zero near the origin and increases smoothly further away, as the tori become more and more "elliptically" asymmetric. The fact that we use spherically symmetric annular regions in no way limits the applicability of our method, since all we seek is to follow faithfully changes in the morphology of the motion as we move away from the origin and that can be accomplished by annular shells of any shape.

Let us elaborate somewhat on the dynamical aspects of our approach: First, by resonances we refer to periodic orbits, which arise in pairs, one stable and one unstable. Here, we concentrate on the

* Corresponding author at: Computational Intelligence Laboratory (CI Lab), Department of Mathematics, University of Patras, GR-26110 Patras, Greece. Tel.: +30 2610 997374; fax: +30 2610 992965.
E-mail address: vrahatis@math.upatras.gr (M.N. Vrahatis).

stable ones, which are surrounded by "islands" of invariant tori [1]. As soon as the annular region mentioned above enters such an island, $D(r)$ jumps discontinuously to a larger value, as the orbits suddenly reach considerably larger distances (determined by the furthest points of the orbits in the islands), while their minimum distances from the origin are similar to what they were before. Enlarging the radii of the shells, $D(r)$ might be expected to decrease somewhat near the center of the island and then increase again as we approach the furthest points of the islands.

As we are plotting, though, the *maximum* value that $D(r)$ can attain every time, the passage through the unstable points of the resonance keeps its value unchanged and is recorded in our graphs as a "plateau". When our shells exit the domain of the islands and enter again a region of tori surrounding the origin, $D(r)$ resumes its smoothly increasing behavior. Thus, plateaus provide information about the location and approximate width of resonance islands. Since our methodology implicitly identifies the very *existence* of resonances, it can also be used to provide evidence whether a given conservative map is completely integrable or not, since resonances (especially their simultaneous presence in the form of chains of different numbers of islands) are generally observed only in non-integrable maps.

Evolutionary Algorithms (EAs) [5,6], are used to accomplish the above optimization task. As is well known, EAs are stochastic algorithms for global optimization inspired by the biological evolution of living organisms using analogous ideas in the setup of their algorithmic approach. They first identify a set of possible solutions of the problem and then evolve them to reach the global optimum solution. In doing this, EAs use such mechanisms as recombination (or crossover), mutation and selection as well as an objective function to evaluate the "fitness" of every current solution identified. Here, we make use of the Differential Evolution (DE) algorithm [7,8], which is a member of the class of EAs and, in general, appears to perform with high efficiency and accuracy.

The Letter is organized as follows. In Section 2 the differential evolution is presented. In Section 3 our proposed methodology is described while Section 4 contains numerical results for 2 and 4-dimensional symplectic maps, coming from the application of the proposed methodology. The Letter ends in Section 5 by presenting concluding remarks.

2. Differential evolution algorithm

Differential Evolution (DE) is a population-based algorithm for global optimization of multimodal functions. It attains a set of possible solutions and evolves them in order to find the "best" one (optimum) among them, according to a well defined set of criteria. The set of possible solutions is called the population of the DE. Some of the advantages of the DE algorithm are the following: (a) It can operate on non-differentiable and/or discontinuous functions of arbitrary dimensions. (b) It can be applied to functions contaminated by noise or functions that change dynamically over time. (c) It can be used to study integer, discrete and mixed programming problems. (d) It can be easily computer-parallelized.

Specifically, the DE algorithm is said to exploit a population of individuals (N-dimensional vectors). Let u_i denote the ith individual of the population. Then, DE is composed of the following four steps:

Step 1. **Initialization step.** Initialize randomly the individuals of the population. Set the mutation factor, F, and the recombination (cross-over) factor, CR, to fixed values within the interval [0, 1] and choose an *objective function* for the problem under study.

Step 2. **Mutation step.** Mutate each individual u_g^i (called the target individual) of the population to form a trial vector, v_{g+1}^i, by applying the following DE algorithm:

$$v_{g+1}^i = u_g^{r1} + F\left(u_g^{r2} - u_g^{r3}\right) + F\left(u_g^{r4} - u_g^{r5}\right), \qquad (1)$$

where $r1$, $r2$, $r3$, $r4$, $r5$ are randomly chosen integers numbering the individuals in the population, such that $r1 \neq r2 \neq r3 \neq r4 \neq r5$ and F is a mutation factor.

Step 3. **Recombination (Crossover) step.** For every element of the trial vector, v_{g+1}^i, obtain a random value, $r \in [0, 1]$. If $r \leqslant CR$, set $u_{g+1}^i = v_{g+1}^i$, otherwise set $u_{g+1}^i = u_g^i$.

Step 4. **Selection step.** For every individual of the population u_{g+1}^i evaluate its value through the objective function. If this value is better than the one of the target individual u_g^i, then the individual u_{g+1}^i replaces the target individual in the next generation of the algorithm. Otherwise, the target individual is retained in the next generation of the DE algorithm. If the termination criterion is not satisfied, then go to the second step. As a termination criterion we can use a predefined number of generations or an error goal value for the objective function.

Of course, there are several other types of DE algorithms similar to (1) [9,10]. However, they generally involve fewer than 5 rk parameters and when we did implement some of them we found that they did not perform any better than (1). Regarding our choice of the mutation factor F and the recombination factor CR, we have found that large values of F produce populations with greater diversity and hence slow down convergence of the DE algorithm, while CR values close to 1 produce new trial points that differ significantly from the previous ones. Choosing $F = 0.5$ and $CR = 0.5$ gave results that were close to optimal and thus we kept this choice for all our experiments. We stress that by convergence we mean that the value of $D(r)$ is stabilized to 4–5 significant digits. Finally, selecting 20 individuals within our spherical shells is dictated by the need to optimize convergence requirements and keep computation times to a minimum. We did, of course, run experiments with population sizes of 30 and 40 individuals and the results for $D(r)$ were quite similar, while computation times were significantly higher.

3. Proposed methodology

Let us now introduce the methodology for the systematic detection of resonances in 2-dimensional maps, since the generalization to the multi-dimensional case is straightforward: We begin with a central elliptic fixed point of a conservative map T, which is either a stable equilibrium, or belongs to a stable m-periodic orbit of T (hence a fixed point of the map T^m), which for convenience we shift to the origin. Concentric circular shells are then generated with increasing radii $r_1 < r_2$ about this point, with small thickness ($r_2 - r_1 \simeq 0.001$ up to 0.005). The aim is to find an initial condition in the interior of the annular region enclosed by two such circles, whose orbit has the maximal difference between the maximum and minimum distance measured from the central elliptic point. By doing this, we convert the prescribed problem to the solution of a maximization problem and make use of the DE algorithm presented in Section 2.

The population of the DE, in this case, is a set of points initialized randomly within concentric circular regions about the origin. The computation of the objective function, for all individuals of the DE, relies on the following procedure: Consider the individual as an initial condition of the map and iterate it for thousands of iterations. Then, compute the maximum and minimum distances between the generated orbit and the central elliptic point. The difference between these two distances is the value of the objective
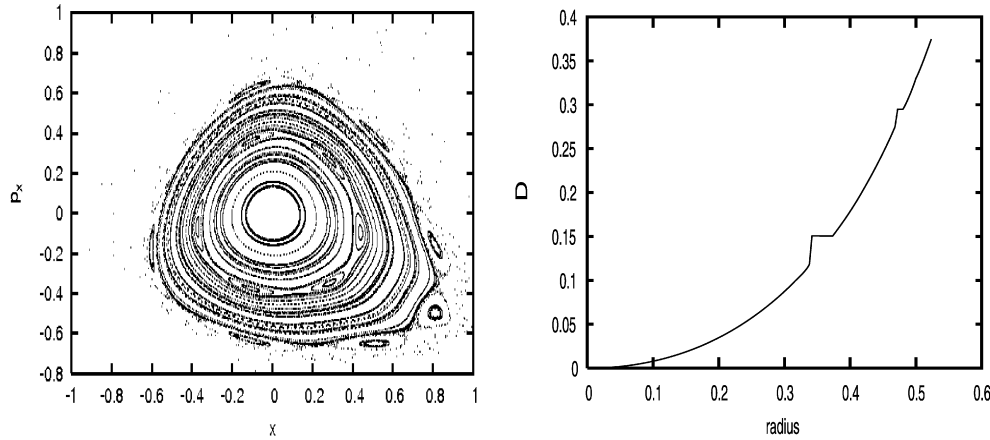
Fig. 1. The phase space of Hénon map with $v_x = 0.175$ is presented in the left panel. On the right D is plotted versus r for the same value of v_x, up to about 0.5, beyond which lies the chaotic domain, where it fails to converge and becomes unbounded.

function which we shall denote as D. The population of the DE is then evolved following the steps of the algorithm described in Section 2. The output of the DE algorithm is a new individual which has the current maximum value of D. The same procedure is then carried out for all regions located between consecutive circles, covering in this way all of phase space. At the end, we output the results of the above methodology by plotting D versus the distance from the origin r.

Simple inspection of the plot generated provides useful evidence regarding the existence of resonances of the map under study. As we will see in Section 4, small "plateaus" on the graph of D versus r, indicate the regions of phase space of the map where resonances may be located. Every time we find such behavior we focus on the particular part of the plot, seeking to magnify its detailed structure. Iterating then the corresponding initial conditions together with those of other neighboring points yields additional information about the location and shape of these resonances in phase space.

Finally, we suggest that this methodology may also be used as a numerical indicator of whether a given map is integrable or not. For example, if our plot reveals a smooth, monotonously increasing function $D(r)$, without any sign of plateaus, this may serve as a strong indication of the integrability of the map.

4. Applications to 2- and 4-dimensional maps

We have applied the methodology described above to several examples of 2- and 4-dimensional maps. In all experiments we select a population of 20 points (initial conditions) and set factors F and CR equal to 0.5. Using the DE operator (1) everywhere in the Letter, each map was iterated for 10^4 iterations.

4.1. The 2-dimensional case

In the experiments of this section we have used the following five maps:

(a) The 2-dimensional Hénon map [11–14], given by:

$$x' = \cos(2\pi v_x)x + \sin(2\pi v_x)(p_x + x^2),$$
$$p'_x = -\sin(2\pi v_x)x + \cos(2\pi v_x)(p_x + x^2),$$

(b) The standard map [2,15]:

$$x' = \left(x + y - \frac{k}{2\pi}\sin(2\pi x)\right) \mod \frac{1}{2},$$

$$y' = \left(y - \frac{k}{2\pi}\sin(2\pi x)\right) \mod \frac{1}{2},$$

(c) The McMillan map [16,17]:

$$x' = y,$$
$$y' = -x + (2\mu y)/(1 + y^2),$$

(d) The product map [18]:

$$x' = (x + 1/x)(1/y),$$
$$y' = x,$$

(e) And finally the Cohen map [19] given by the equations:

$$x' = \sqrt{1 + x^2} - y,$$
$$y' = x.$$

The 2-dimensional Hénon map is a well-known non-integrable symplectic map, which can be used to describe the 2-dimensional betatronic motion in a magnetic lattice of an accelerator machine: (x, p_x) are the so-called Courant–Snyder coordinates and the linear part of the map is a rotation by a constant angle $\omega = 2\pi v_x$ [11,13,14]. The standard map is also symplectic with large scale chaotic behavior becoming evident as $k > 0$ grows [2]. It is integrable only for $k = 0$, since in that case the map is linear. On the other hand, the McMillan map is known to be integrable for all values of its parameter μ, possessing a family of invariant curves given by $I(x, y) = x^2y^2 + x^2 + y^2 - 2\mu xy$ [16,17], while it is not yet known whether the product and Cohen maps are integrable or not. What has only been proven is that the Cohen map does not posses a first algebraic integral [19].

Concerning the radial steps taken in each map for the application of our method, their length for the Hénon map was taken equal to 0.005, for the standard map and the Cohen map was 0.003 while for the McMillan map and the product map the radial step was equal to 0.002.

In the left panel of Fig. 1 the phase space of Hénon map with frequency $v_x = 0.175$ is presented and the corresponding plot of D versus the radial distance r from the origin is exhibited on the right panel. It is clear that near the approximate radii 0.35 and 0.48 small "plateaus" are observed. After the value of the radius becomes 0.5, the orbit enters in the chaotic regions of the map, oscillates wildly at first and then escapes to infinity after a small number of iterations. These plateaus correspond to two chains of islands of period 6 and 13 that appear in Fig. 2. These islands were
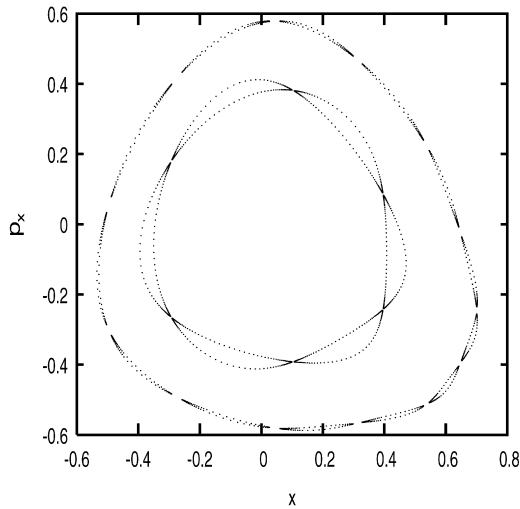
Fig. 2. The two chains of islands found in Hénon map with $v_x = 0.175$ by iterating the map using as initial conditions points that appear at the plateau at radii 0.35 and 0.48 of the right panel of Fig. 1. The initial conditions for these island chains respectively are ($x = -0.27996935$, $y = 0.20451539$) and ($x = -0.35738108$, $y = 0.31484934$).
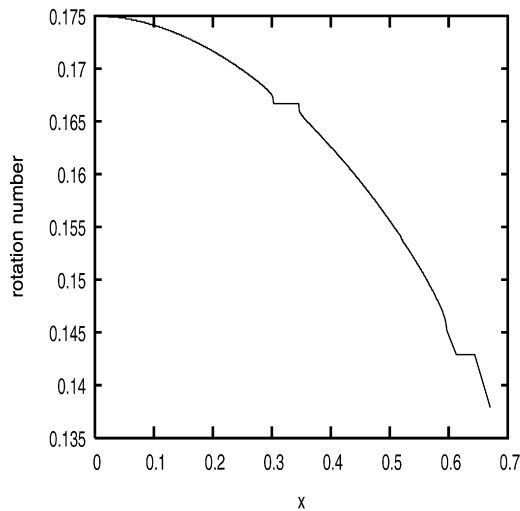

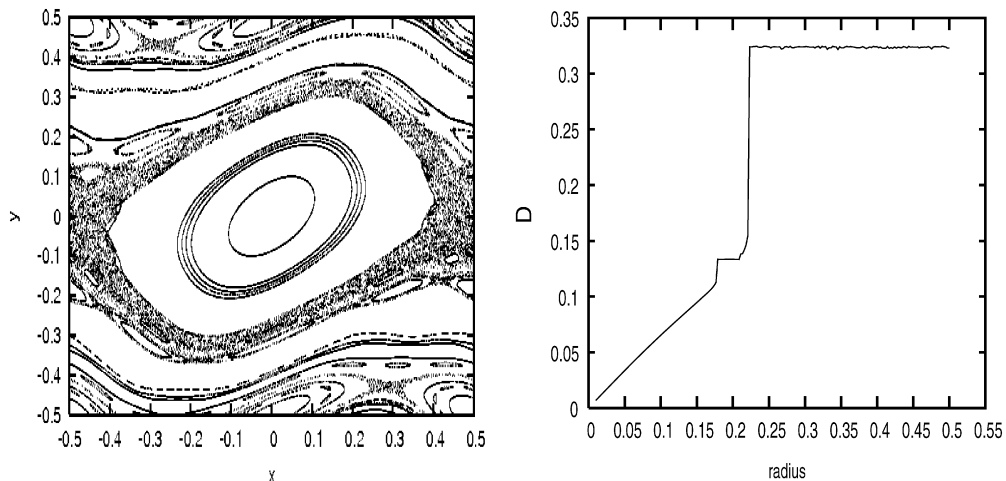**Fig. 3.** The plot of the rotation number for Hénon's map with $v_x = 0.175$.

computed by iterating the Hénon map, with $v_x = 0.175$, using as initial conditions the output points found by the DE algorithm for $r = 0.35$ and 0.48 (see the caption of Fig. 2).

In Fig. 3 we plot the rotation number [15] for Hénon's map with $v_x = 0.175$, as a function of the distance from the origin, moving along the $y = -x$ direction with a small step and executing iterations of the map. The rotation number σ is defined by the limit

$$\sigma = \lim_{n \to \infty} \frac{1}{n} \sum_{i=1}^{n} \theta_i,$$

where θ_i are successive angles produced at every iteration i on the plane of the map and represents the average angle between the produced points and the central point of the map. As is well known, for periodic orbits the rotation number is equal to the ratio of two positive integers, for quasiperiodic orbits it is irrational and is not defined for a chaotic orbit. Proceeding outwards from a central elliptic point, we find that σ is a smooth, monotonous function of the radial distance r and generates small plateaus at locations where islands of periodic orbits appear.

We notice that this approach does recognize the first chain of islands with rotation number 1/6 as well as the last one with rotation number 1/7 but fails to identify (using the same step size 0.005 as in the DE algorithm), the chain of islands in between with rotation number 2/13 found by our methodology. When we did decrease the step size to 0.001, the rotation number detected the 2/13 resonance, indicating its lower sensitivity compared to our approach. The most serious disadvantage, however, is that the rotation number does not readily extend to the case of more than 2 dimensions.

Next, we apply our method to the standard map and plot D versus the radial distance from $(0, 0)$ in Fig. 4. The radial step size used was equal to 0.003. The first plateau is located close to a distance approximately 0.18 from the origin. A last big plateau is detected starting with radius 0.22 which means that all orbits in that region have almost the same value of D. Thus, if we use as initial condition the output point found by the DE algorithm at radius 0.19 (with $x = -0.03810525$, $y = 0.18686112$) and the one at a radius 0.23 (with $x = -0.16142492$, $y = 0.16315651$) and iterate them through the standard map 10^3 times, we get two chains of islands of regular motion presented in Fig. 5 with rotation numbers 1/8 and 1/10.

In Fig. 6, on the other hand, we observe that the plot of D versus r for the McMillan map yields a smooth curve with no plateaus or fluctuations, until the radius reaches the outer part of the phase space of the map. As we mentioned before, this map is known to

Fig. 4. The phase space of the standard map with $k = 0.9$ is presented in the left panel, while on the right D is plotted versus r for the same value of k. Note that, after forming the second plateau, D ceases to converge and exhibits small fluctuations, as the orbits enter the large chaotic "sea" surrounding the central regular region.

be integrable and free from resonance islands. This is corroborated by the fact that the plot produced by the proposed methodology
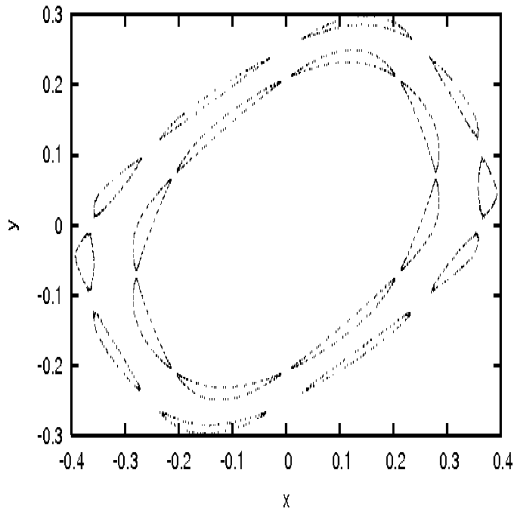
shows that there are no visible resonances and hence provides strong evidence for the integrability of the map.

Finally, Figs. 7 and 8 correspond to the product and the Cohen maps, respectively. On the right panel of Fig. 7, the plot does not give any indication for the existence of resonances in the phase space and hence suggests that the product map is integrable. Our results about the Cohen map are even more interesting: The plot produced by the DE algorithm is presented in Fig. 8. Note that, in the magnification of the right panel of Fig. 8 shown in Fig. 9, two chains of islands with periods 14 and 23 are discovered very close to radii 1 and 1.58 respectively. If we use as initial conditions the "best" points found by the DE algorithm at radius 1 ($x = 1.38551745$, $y = 0.01315274$) and radius 1.58 ($x = -0.11757663$, $y = 1.99341441$) and iterate them through the Cohen map 10^3 times, we indeed locate these islands as displayed in Fig. 10.

A further study of the resonances identified in Fig. 9 reveals the presence of saddle points with eigenvalues very close but not equal to 1. In particular, for the period 14 orbit we find that the saddle point is located at $x \approx 1.23590433$, $y \approx 1.80320245$ with eigenvalues $\lambda_1 \approx 1.01226$, $\lambda_2 = 1/\lambda_1 \approx 0.98789$, while for the period 23 we find that the saddle point $x \approx 1.64966043$, $y \approx 2.76893060$ has eigenvalues $\lambda_1 \approx 1.01227$, $\lambda_2 = 1/\lambda_1 \approx 0.98788$. The rotation numbers are 3/14 and 5/23 while the corresponding elliptic points are located at $x = 0.02582572$, $y = -0.39650893$ and $x = -0.06696497$, $y = 2.01814322$.

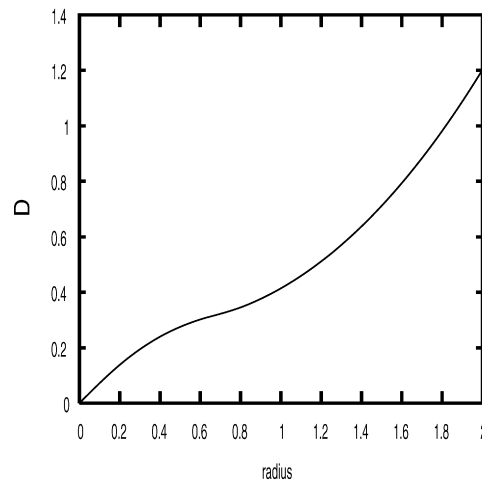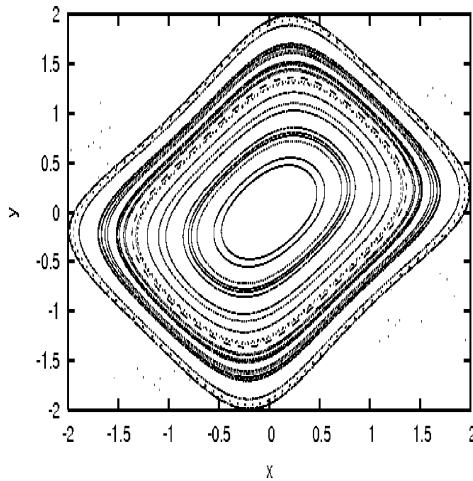**Fig. 5.** Chains of islands found for the standard map with $k = 0.9$, using as initial conditions points appearing at the beginning of the plateaus at radii 0.19 and 0.23 of Fig. 4.

Fig. 6. The phase space of the McMillan map with $\mu = 0.5$ is presented in the left panel and on the right D is plotted versus r for the same μ.
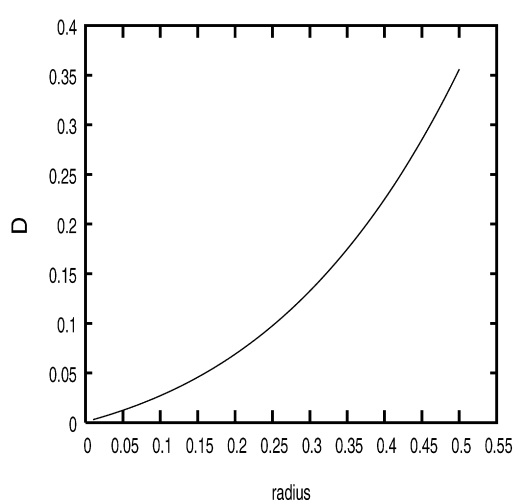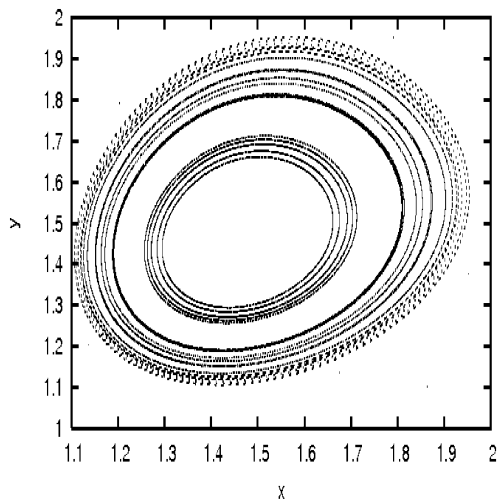

Fig. 7. The phase space of the product map is presented in the left panel, while on the right D is plotted versus r for the same map.
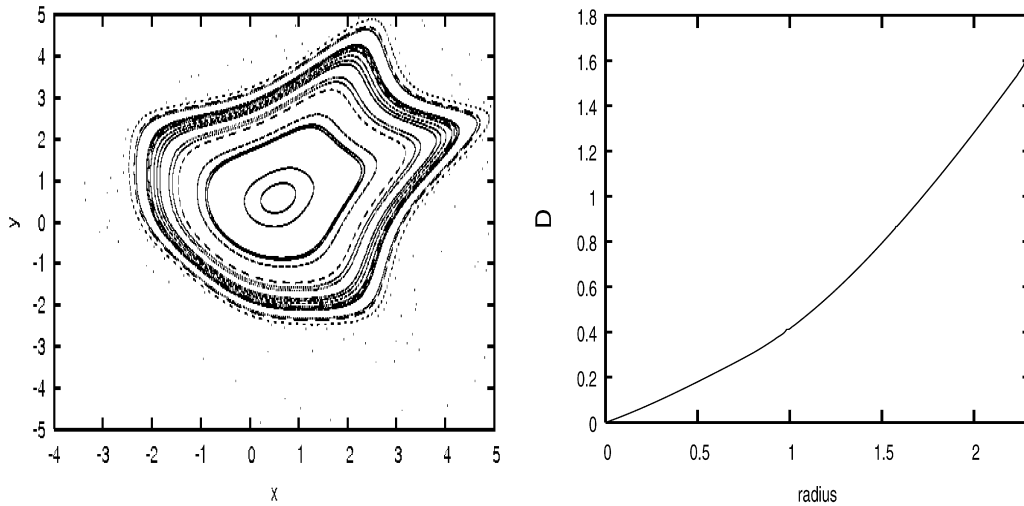
Fig. 8. The phase space of the Cohen map is presented in the left panel and in the right panel the plot of D versus radius for the same map.
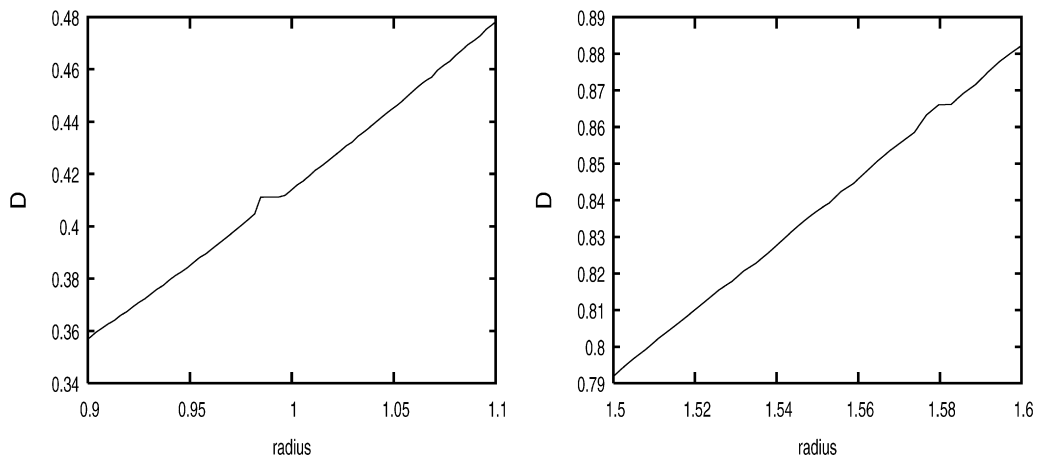

Fig. 9. A magnification of the right panel of Fig. 8 close to radius 1 is presented in the left panel showing the plateau corresponding to the 3/14 orbit, while in the right panel a magnification of the right panel of Fig. 8 near radius 1.58 is shown demonstrating the presence of the 5/23 resonance.
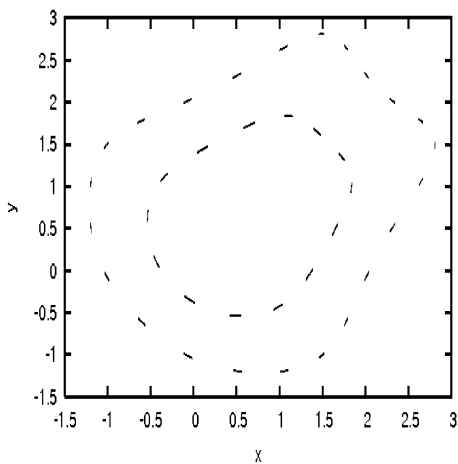

Fig. 10. The two chains of islands found in the Cohen map using as initial conditions points that appear at the two plateaus of the Fig. 9.

These results strongly suggest that the Cohen map is not integrable in the sense that it possesses multiple resonances, near the saddle points of which one expects to find chaotic behavior precluding the existence of a one parameter family of invariant curves describing the global dynamics of the map.

Regarding computation times, e.g. in the case of Hénon's map, where we proceeded in 20 directions with 50 iterations of the DE algorithm in each direction, our calculations required approximately 15 min. On the other hand, the rotation number plot of Fig. 3 (where one proceeds in only one direction), takes 5 min for 1000 steps, with 10^5 iterations at each step to achieve convergence. Thus, it is clear that if we wanted to strengthen the rotation number results by proceeding in more directions, computation times would quickly exceed those needed for the DE algorithm.

4.2. The 4-dimensional case

Let us now apply our methodology to the 4-dimensional Hénon map [11–13] given by the equations:

$$x' = \cos(2\pi \nu_x)x + \sin(2\pi \nu_x)\left(p_x + (x^2 - y^2)\right),$$

$$p'_x = -\sin(2\pi \nu_x)x + \cos(2\pi \nu_x)\left(p_x + (x^2 - y^2)\right),$$

$$y' = \cos(2\pi \nu_y)y + \sin(2\pi \nu_y)(p_y - 2xy),$$

$$p'_y = -\sin(2\pi \nu_y)y + \cos(2\pi \nu_y)(p_y - 2xy),$$

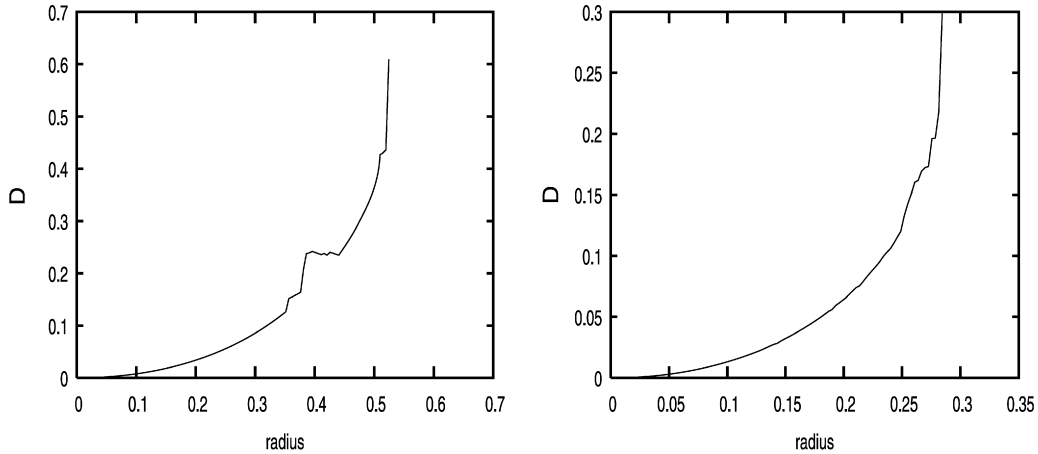as well as to a 4-dimensional McMillan map [20] given by the equations:

Fig. 11. The plot of D versus radius for the 4-dimensional Hénon map with frequencies $v_x = 0.61903$, $v_y = 0.4152$ is presented in the left panel and in the right panel we show the plot of D versus radius for the same map with frequencies $v_x = 0.28$, $v_y = 0.31$.

$$x'_1 = x_2,$$
$$x'_2 = -x_1 + 2kx_2/(x_2^2 + y_2^2 + 1) + \varepsilon x_2,$$
$$y'_1 = y_2,$$
$$y'_2 = -y_1 + 2ky_2/(x_2^2 + y_2^2 + 1) + \varepsilon y_2.$$

The 4-dimensional Hénon map describes the effects of a particle's motion through nonlinear magnetic focusing elements of the FODO cell type [11–14]. The x, y variables are deviations of the particle's motion from the ideal circular trajectory in the horizontal and vertical direction respectively and p_x, p_y are the corresponding momenta. Variables v_x, v_y are the so-called tune parameters of the accelerator machine. For this application, we have used the pairs of frequencies $v_x = 0.61903$, $v_y = 0.4152$ and $v_x = 0.28$, $v_y = 0.31$ separately. The produced plots resulting from the application of the DE algorithm (where, instead of circles we now use 4-dimensional "spheres" of radius r) are presented in the two panels of Fig. 11. The radius step was set equal to 0.005.

Note, in particular, on the left panel of Fig. 11 that if one starts applying this procedure at a radius of 0.35, the plot presents non-smooth behavior showing several small plateaus up to radius 0.5. Beyond this distance, D oscillates rapidly and then goes to infinity due to the presence of large scale chaos. Similar results are presented on the right panel of Fig. 11, at the other pair of parameter values. Here, the plot loses its smoothness after radius 0.25 and when the radius becomes nearly equal to 0.27 large scale chaos appears.

We then investigated further the 4-dimensional Hénon map, with frequencies $v_x = 0.61903$, $v_y = 0.4152$ and were able to locate the resonances identified by the DE algorithm. More specifically, we found periodic orbits in the neighborhood of a point that corresponds to the plateau on the left panel of Fig. 11 near radius 0.41, one of which has period 32 with initial conditions ($x = 0.38384187$, $p_x = -0.07366717$, $y = 0.00000005$, $p_y = -0.14620234$). Starting near this point we iterated the map 10^4 times and obtained the orbit shown in Fig. 12, which looks like 8 isolated tori. Interestingly enough, when projected on the x, p_x plane, these look like a chain of 8 islands similar to the ones found in the 2-dimensional case.

Finally, in Fig. 13 we exhibit the plot of D versus r for the 4-dimensional McMillan map in the case $\varepsilon = 0$, where it is known to be integrable. The radius step was set to 0.001. We again observe that the curves of the plot are smooth and similar to the ones found for the integrable 2-dimensional McMillan map. However, if we make a small perturbation to the above map, by setting $\varepsilon = 0.1$, the corresponding plot of D versus r shown in Fig. 14 dis-
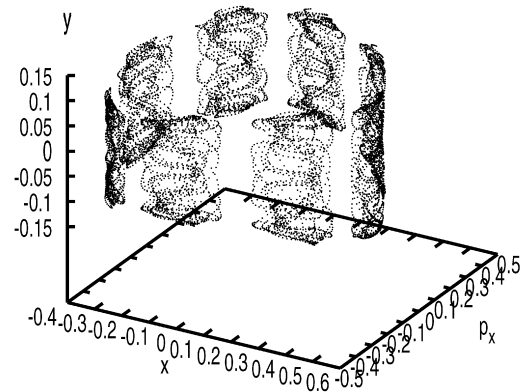

Fig. 12. 8 tori produced by the iteration of a point lying close to a period 32 for the 4-dimensional Hénon map, with frequencies $v_x = 0.61903$, $v_y = 0.4152$.
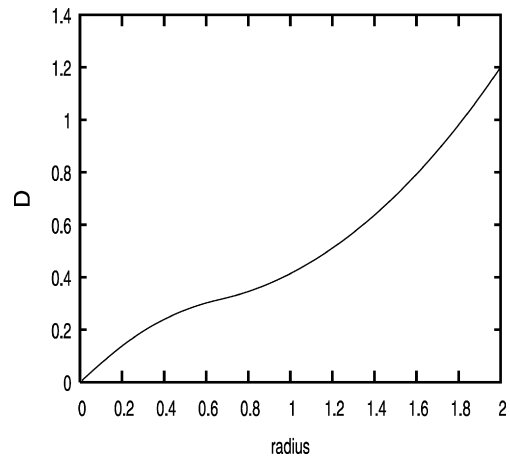

Fig. 13. Plot of D versus radius produced by the proposed methodology for the 4-dimensional McMillan-like integrable map with $k = 0.5$ and $\epsilon = 0$.

plays small plateaus. In this case, the 4-dimensional McMillan map is not expected to be integrable and this is strongly suggested by the four small plateaus appearing in the plot (denoted by the circles around them), providing reliable indication for the existence of resonances of the map.
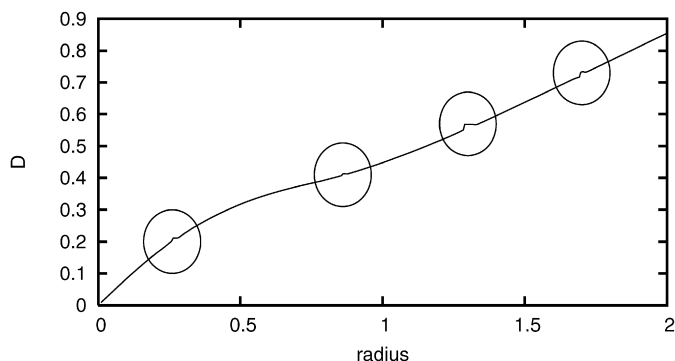
Fig. 14. Plot of D versus r produced by the proposed methodology for the 4-dimensional McMillan-like map, with $k = 0.5$ and $\varepsilon = 0.1$.

5. Conclusions

A new methodology has been proposed for the detection of resonances in conservative maps. It relies on the solution of an optimization problem, uses evolutionary algorithms and can be applied to maps of any dimension. Basically, it introduces a function $D(r)$ of the radial distance r from the origin of the map, whose smoothness and monotonicity reveal important properties concerning the dynamics. In this Letter, we applied this methodology to various examples of 2- and 4-dimensional symplectic maps and obtained interesting results showing the effectiveness of our method in detecting the location and approximate size of resonances, represented by "plateaus" in the graph of $D(r)$ versus r. We also demonstrated an additional aspect of the proposed methodology, i.e. that it can be used to provide evidence regarding the complete integrability of a given map, since completely integrable maps generally do not possess multiple chains of different numbers of resonance islands.

We wish to emphasize that our aim in this work was not to propose a new analytical criterion for studying resonances, similar in rigor and accuracy to other more sophisticated approaches known in the literature [21–23]. Rather, our purpose was to present a new practical technique for locating all resonance islands within a prescribed level of resolution, which is efficient, relatively fast and applies to multi-dimensional conservative dynamical systems. It is clear that a solid mathematical basis for our method is still lacking. Still, encouraged by the results presented here, we believe that the search for such a justification is worth pursuing in a future publication.

References

[1] M.A. Lieberman, A.J. Lichtenberg, Regular and Chaotic Dynamics, Springer-Verlag, 1992.
[2] R.S. MacKay, J.D. Meiss (Eds.), Hamiltonian Dynamical Systems, Adam Hilger, Bristol, 1987.
[3] W. Scandale, G. Turchetti (Eds.), Nonlinear Problems in Future Particle Accelerators, World Scientific, Singapore, 1991.
[4] T. Bountis, Ch. Skokos, Nucl. Instrum. Methods Phys. Res. Sect. A 561 (2006) 173.
[5] T. Back, Evolutionary Algorithms in Theory and Practice: Evolution Strategies, Evolutionary Programming, Genetic Algorithms, Oxford Univ. Press, 1996.
[6] T. Back, D. Fogel, Z. Michalewicz, Handbook of Evolutionary Computation, Oxford Univ. Press, 1997.
[7] D. Corne, M. Dorigo, F. Glover, New Ideas in Optimization, McGraw–Hill, London, 1999.
[8] R. Storn, K. Price, J. Global Opt. 11 (4) (1997) 341.
[9] D.K. Tasoulis, V.P. Plagianakos, M.N. Vrahatis, Clustering in Evolutionary Algorithms to Efficiently Compute Simultaneously Local and Global Minima, Congress on Evolutionary Computation (CEC 2005), vol. 2, 2005, pp. 847–1854.
[10] M.G. Epitropakis, V.P. Plagianakos, M.N. Vrahatis, Balancing the exploration and exploitation capabilities of the differential evolution algorithm, in: IEEE Congress on Evolutionary Computation (CEC 2008), Hong Kong, June 2008.
[11] E. Todesco, M. Giovannozzi, Phys. Rev. E 53 (4) (1996) 4067.
[12] M.N. Vrahatis, H. Isliker, T.C. Bountis, Int. J. Bifur. Chaos 7 (12) (1997) 2707.
[13] A. Bazzani, E. Todesco, G. Turchetti, G. Servizi, A normal form approach to the theory of nonlinear betatronic motion, CERN, Yellow Reports, 94-02, 1994.
[14] M.N. Vrahatis, J. Comput. Phys. 119 (1995) 105.
[15] J.D. Meiss, Rev. Mod. Phys. 64 (3) (1992) 795.
[16] E.M. McMillan, A problem in the stability of periodic systems, in: E. Britton, H. Odabasi (Eds.), Topics in Modern Physics. A Tribute to Condon E.U., Colorado Univ. Press, Boulder, CO, 1971, pp. 219–244.
[17] M.L. Glasser, G.V. Papageorgiou, T.C. Bountis, SIAM J. Appl. Math. 49 (3) (1989) 692.
[18] Private communication with V.G. Papageorgiou.
[19] M. Rychlik, M. Torgerson, New York J. Math. 4 (1998) 57.
[20] T. Bountis, A. Goriely, M. Kollmann, Phys. Lett. A 206 (1995) 38.
[21] J. Laskar, Icarus 88 (1990) 266.
[22] G. Contopoulos, N. Voglis, Astron. Astrophys. 317 (1997) 73.
[23] L. Vela-Arevalo, J.E. Marsden, Class. Quantum Grav. 21 (2004) S351.